Clues to Understanding the Enigma of the Unusual Asterism in 'Mercedes-Star' Quartz

Jean-Pierre Gauthier, Emmanuel Fritsch, Thanh Nhan Bui, Jacques Fereire

Clues to Understanding the Enigma of the Unusual Asterism in 'Mercedes-Star' Quartz

Jean-Pierre Gauthier, Emmanuel Fritsch, Thanh Nhan Bui and Jacques Fereire

ABSTRACT: 'Mercedes-star' quartz contains abundant long, narrow, randomly oriented rutile inclusions, and is notable for its unusual asterism. In particular, it displays weak three-rayed stars, with rays that meet at the centre as in the Mercedes-Benz emblem. In the classical theory of asterism such stars cannot exist, and they have not been seen in any other gem materials. We examined three samples (two spheres and an egg) of 'Mercedes-star' quartz from Brazil. Ideally, this material displays six three-rayed stars located along two latitude planes parallel to the equatorial plane (perpendicular to the *c*-axis). In addition, six faint four-rayed stars are located along the equatorial plane. Therefore, in total, this quartz may display 18 stars located on three coaxial circles. The rays of all the stars consist of a path of reflective segments of unknown illumination origin, but which appear to result from double reflection of the light beam, first by Brazil-law twin planes and then by the rutile needles, making the phenomenon uncommon. In addition to the abovementioned stars seen in reflected light (epiasterism), more-transparent 'Mercedes-star' quartz may also show two six-rayed stars with transmitted light (diasterism) when illuminated from behind and viewed parallel to the *c*-axis.

INTRODUCTION

Quartz is one of the most abundant minerals on Earth. It occurs in many varieties, not just colour-wise (e.g. amethyst, citrine, prasiolite, pink quartz and smoky quartz) but also inclusion-wise (Hyršl & Niedermayr 2003). Of all quartz inclusions, rutile is relatively common, and it occurs in some spectacular varieties (e.g. Gübelin & Koivula 2005, pp. 627–631). Many of these are artistically highlighted by lapidaries.

Several types of inclusions are responsible for various optical phenomena in gems, such as aventurescence, iridescence, chatoyancy and asterism. Chatoyancy in quartz is produced by a network of parallel acicular inclusions oriented along a particular crystallographic direction of the quartz host (see, e.g., Kane 1985; Koivula 1987; Choudhary & Vyas 2009). Relatively parallel coarse rutile needles sometimes produce pseudo-cat's-eyes (Johnson & McClure 1997). The asterism is typically caused by several networks of acicular inclusions lying in the basal plane that produce six-rayed stars and, less frequently, 12-rayed stars (Johnson & Koivula 1999). Additional inclusion networks outside the basal plane result in multi-asterism, mainly consisting of four- and six-rayed stars (Schmetzer & Glas 2003).

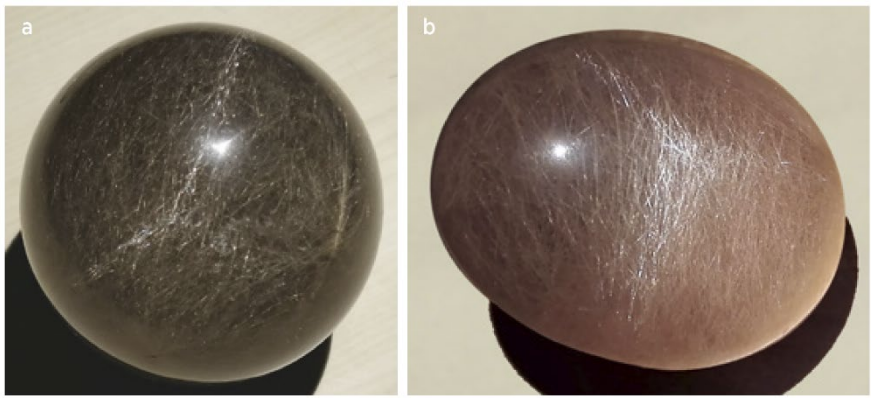

Figure 1: These two samples of Mercedes-star quartz were examined for this study: (a) a large sphere (1,470 ct; 60 mm in diameter) and (b) an egg (252.5 ct; 41 mm long × 60 mm in diameter). Collection of E. Fritsch; photos by J.-P. Gauthier.

Here we examine so-called Mercedes-star rutilated quartz (e.g. Figure 1), which displays three-rayed asterism with branches that meet at the centre of the star (like the emblem of the famous German automaker), and exhibits features that are contrary to the most commonly accepted theory of asterism (cf. Gübelin *et al.* 1982; Weibel 1982). This kind of asteriated quartz was briefly described by Gübelin and Koivula (2005, pp. 548, 822) and later encountered by Hainschwang (2007) in five samples from Brazil. More recently, it was reported by Steinbach (2017), as well as Schmetzer and Steinbach (2022, 2023), in rutilated quartz also from Brazil (apparently similar to the samples described here). The arrangement of the stars located at various positions relative to the optic axis of the host quartz is documented in the present article using three spherical or egg-shaped specimens of rutilated quartz from Brazil, which in one case was sacrificed to study the cause of the three-rayed asterism. We report a number of observations not previously described for Mercedes-star quartz, and also propose some clues to explain the formation of its unique asterism.

MATERIALS AND METHODS

The three Mercedes-star quartz samples examined for this study all came from Bahia State, Brazil. The first was an opaque sphere of 60 mm diameter (1,470 ct; Figure 1a). This sample was used for most of the observations, because the stars were easiest to see and all were visible. The second was an egg measuring 41 mm long × 30 mm diameter (252.5 ct; Figure 1b), which was semi-transparent in transmitted light, making it ideal for observing any diasterism. The third sample was a 28-mm-diameter sphere that was somewhat translucent, due in particular to its smaller size (150 ct; Figure 2). This last sample was sliced to prepare petrographic thin sections for observation between crossed polarisers.

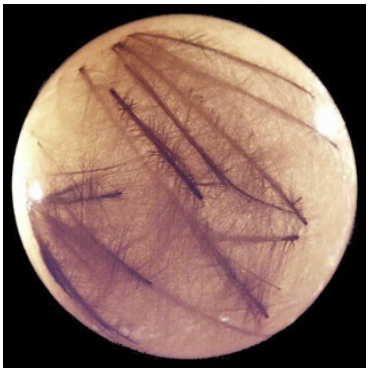

Figure 2: A smaller Mercedes-star quartz sphere measuring 2.8 cm in diameter was also examined for this study, and is shown here in transmitted light to highlight the interesting form of its inclusions. Photo by J.-P. Gauthier.

To describe the asterism in our samples, it was necessary to develop a protocol to locate the centres of all the stars. The following process was done using the large sphere (Figure 1a): First, the light source (such as the sun) and the observer faced the same direction. In this orientation, the specular reflection (the image of the light source reflected by the surface of the sphere as seen by the observer) was approximately in the centre of the spherical surface (Figure 3a). Then, the centre of a star was moved (by rotating the sphere) to coincide with this specular reflection (Figure 3b), and a small disc of paper was affixed to indicate this position (Figure 3c). This was done for the centre of each star. For the purpose of this study, these positions of the star centres are called *star spots*. They should not be confused with *light spots*, as previously described for star rose quartz spheres (e.g. Schmetzer and Krzemnicki 2006; Killingback 2008).

The relative angular positions of the star spots on the large sphere were then recorded with a Tri-Mesures MC 1004E three-dimensional coordinate measuring machine (manufactured by Metrovali, Villedieu-sur-Indre, France) equipped with Wenzel WM/Quartis metrological software. Experimentally, five non-coplanar points on the sphere first defined the sphere's centre (denoted Ω). The coordinates of each star spot were obtained in relation to this origin. The next step was to calculate the coordinates of the north pole (P) and the south pole (P') of an axis passing through the diameter of the sphere, making it possible to evaluate the angular positions of the spots. (Note: Due to the positional symmetry of the spots as described below, the quartz *c*-axis was determined and chosen as the reference axis P–P'.) We could then calculate the angular positions (with respect to the *c*-axis and/or the equatorial plane) of the

radii joining the sphere centre Ω to the different star spots. Due to uncertainty in positioning the star spots (discussed further below), the angular values were rounded to the nearest half degree.

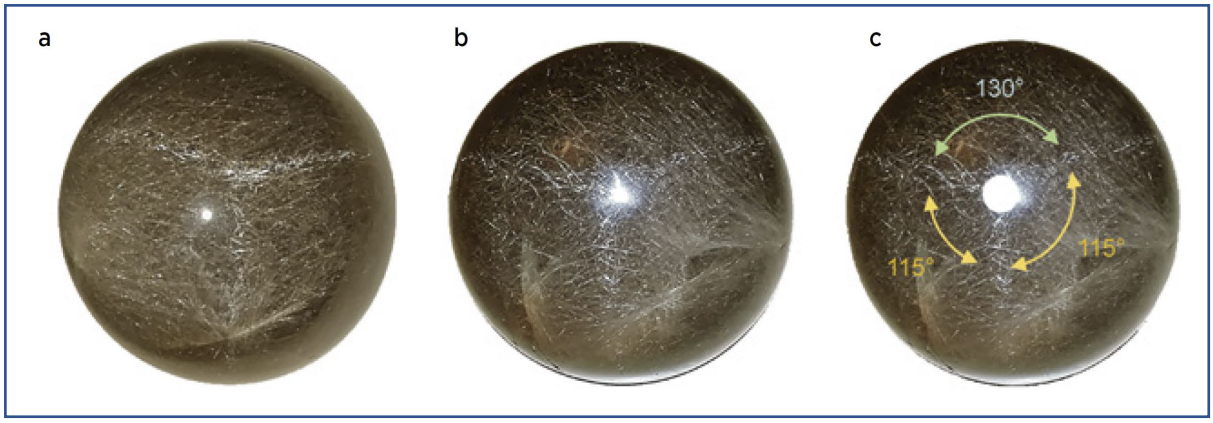

Figure 3: The positions of 'star spots' on the large quartz sphere were determined as follows: (a) First the light source and the eye of the observer are aligned with the sphere's centre, so the specular spot becomes centred on the sphere. (b) Then the sphere is rotated slightly to bring the centre of a star in coincidence with the specular spot. (c) The position of the star spot is marked with a disc of sticky paper. Angle values between branches are about 130° (white arrows) and 115° (yellow arrows). Photos by J.-P. Gauthier.

To identify the acicular inclusions in the quartz, we used a Jobin Yvon T64000 high-resolution Raman spectrometer coupled with an Olympus binocular microscope (up to 100× magnification). With 514 nm excitation from an Ar^+ laser, we employed a triple-subtractive configuration to eliminate the effect of the excitation line, along with a diffraction grating (600 lines/mm), confocal mode and a resolution of approximately 4 cm^{-1}.

RESULTS

Macroscopic Observations

General Features of the Asterism. Viewed in reflected light, eighteen star spots were identified on the large quartz sphere, which were distributed on three coaxial circles (Figures 4 and 5a). A set of six four-rayed star spots lay along the median ('equatorial') plane, and two symmetric sets of three-rayed star spots were located along parallel ('latitude') planes on either side of this equatorial plane. This arrangement strongly suggests that the normal to all of these circles is the quartz *c*-axis (optic axis), which is vertical in Figures 4a and 5, and perpendicular to the plane of the photo in Figure 4b. This could not be verified directly on the large sphere, which was much too thick to be transparent between crossed polarisers, but it was later confirmed using the small sphere (see below).

The appearance of the three-rayed stars in Mercedes-star quartz stands out because of two main characteristics when compared with typical asterism. (1) As seen in Figures 1 and 3, each ray of the star seems to be made of a multitude of reflective points or segments. The branches are relatively wide and diffuse—appearing as shiny, intermittent lines made up of reflections from rutile needles—rather than continuous, sharp and linear rays as in star corundum, for example. (2) The branches of the three-rayed stars meet at a central point, rather than crossing each other to form a classic six-rayed star.

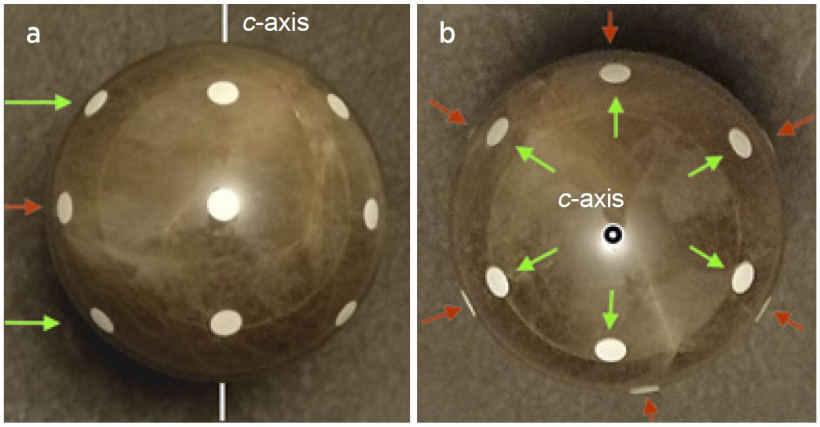

Figure 4: (a) When the large quartz sphere is positioned with the quartz three-fold *c*-axis lying in the plane of the figure, there are six three-rayed stars in the upper and lower hemispheres (green arrows) and six four-rayed stars along the equatorial plane (red arrow). These three sets lie on three parallel circles with their axes collinear with the *c*-axis of the quartz. (b) A view along the quartz three-fold *c*-axis shows the arrangement of six star spots of the three-rayed stars (green arrows). The star spots of six equatorial four-rayed stars (barely visible around the perimeter of the sphere) are indicated by red arrows. Photos by J.-P. Gauthier.

However, as for every asteriated stone, the stars move when one of the three entities—stone, light source or observer—shifts while the other two are fixed. Rotating the stone causes the branches of the star move in the same direction. However, if the lamp or the observer moves, the star shifts in the opposite direction (cf. Gübelin *et al.* 1982). In addition, the arms of the stars are linked together in a network (Schmetzer & Steinbach 2023) that moves as the stone rotates relative to the light source, as in typical asterism exhibited by a multi-star network, such as seen in garnet (Walcott 1937; Schmetzer & Bernhardt 2002) or quartz (Schmetzer & Glas 2003).

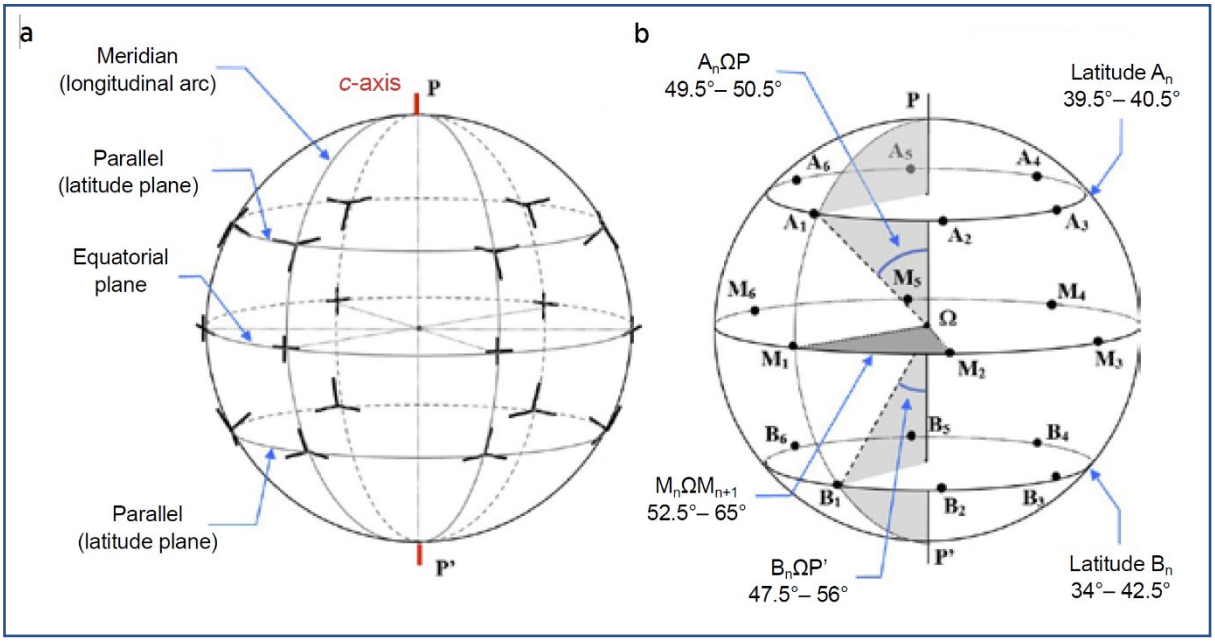

Figure 5: (a) The locations of the 18 star spots seen on the large quartz sphere are shown on this diagram. The labels P and P' show the positions of the north and south 'poles' of the *c*-axis, respectively. (b) A corresponding diagram is labelled with the nomenclature of the star spots relative to their angular positions on meridians (longitudinal arcs connecting the poles) and parallels (or latitude planes) of the quartz sphere. The labels A_n and B_n correspond to three-rayed stars, while M_n refers to the four-rayed stars along the equatorial plane.

Position and Shape of the Stars. The 18 star spots are distributed as follows: six of them are located on each of three parallel circles centred around the same axis, and three of them are on each of six meridians positioned at about 60° of longitude from each other (Figure 5a). Each meridian contains two three-rayed stars opposite in latitude on either side of an equatorial four-rayed star.

Each equatorial four-rayed star has a weak vertical branch (following a meridian) and a much weaker horizontal branch (Figure 6). The lack of visibility of the latter branch is likely the reason why these four-rayed stars were not mentioned in previous publications about Mercedes-star quartz (Steinbach 2017; Schmetzer & Steinbach 2022) until recently (Schmetzer & Steinbach 2023).

Figure 6: The four-rayed asterism on the large quartz sphere is difficult to capture in a photograph. The vertical ray is somewhat visible here, but only part of the horizontal ray is relatively easy to see (yellow arrow). Compare this to the sample in the centre of figure 19 in Hainschwang (2007). Photo by J.-P. Gauthier.

The three-rayed stars have one branch along a meridian (joining the vertical branch of a nearby four-rayed star). The other two branches make an angle of about 115° with the meridian branch and an angle of 130° to one another (Figure 3c). This means that the cause of the meridian branch differs from that of the other two. Of course, there is no need for the Mercedes-star branches to be evenly spaced at 120°, since in quartz there is no three-fold axis of rotation other than the one connecting the two poles (i.e. the *c*-axis, as typical hydrothermal α-quartz is trigonal). The presence of six stars on each of the parallel circles gives a pseudo-hexagonal distribution, reflecting the pseudo-hexagonal symmetry of quartz. This suggests that: (1) the quartz *z* faces are as prominent as the *r* faces, or (2) that twinning has occurred with parallel axes of two trigonal domains inducing the six-fold axis (Frondel 1962).

Table I lists the positional data for the 18 star spots recorded for the large sphere using the three-dimensional coordinate measuring machine. (To identify each star spot, the nomenclature shown in Figure 5b was adopted). The latitude values of the six three-rayed star spots in the 'northern hemisphere' were very similar, with values of 40° ± 0.5°. Those of the southern hemisphere, which would be expected to have symmetrical latitude values, showed greater variation (34°–42.5°). There was also some variation from the expected latitude of 0° for the four-rayed stars along the equatorial plane (0.5°–4.5°). In longitude, the angular spacing between consecutive four-rayed star spots should approach a theoretical value of 60°, but some measurements were quite far away from it, ranging from 52.5° to 65° (again, see Table I).

The deviations from the expected values are probably due to the uncertainty of marking of star spots on the surface of the sphere (estimated at 2–3 mm), and not from the measuring machine (with an uncertainty of about 10 μm). The marked positions of the star spots were imprecise for two reasons. First, the observer's head obscures the sphere unless it is slightly away from the theoretical line defined by the illumination source (e.g. the sun) and the observer in order to see the specular reflection. A similar situation exists if the light source is a lamp placed directly in line between the observer's eye and the sample: The observer will be unable to see the specular reflection unless the sphere is moved slightly to one side of the lamp. Second, the star branches are wide and dotted, so the star spots themselves are not well defined. Due to the resulting inaccuracy in the position of the spots, the angular deviation $\Delta\theta$ with respect to an ideal position can reach up to $\Delta\theta = (\Delta d/R) \times (180/\pi)$ degrees, or about 6° for $\Delta d = 3$ mm (linear

deviation at the surface of the sphere of radius R) and R = 30 mm (as for large sphere) with the constant π= 3.1416.

Angles $A_n\Omega P$	$A_1\Omega P$	$A_2\Omega P$	$A_3\Omega P$	$A_4\Omega P$	$A_5\Omega P$	$A_6\Omega P$
	50	50	49.5	50	50.5	49.5
Latitude of A_n	40	40	40.5	40	39.5	40.5

Angles $B_n\Omega P'$	$B_1\Omega P'$	$B_2\Omega P'$	$B_3\Omega P'$	$B_4\Omega P'$	$B_5\Omega P'$	$B_6\Omega P'$
	51	49	47.5	56	54	53
Latitude of B_n	39	41	42.5	34	36	37

Angles $M_n\Omega P$	$M_1\Omega P$	$M_2\Omega P$	$M_3\Omega P$	$M_4\Omega P$	$M_5\Omega P$	$M_6\Omega P$
	89.5	89	88.5	88	85.5	86.5
Latitude of M_n	0.5	1	1.5	2	4.5	3.5

Angles $M_n\Omega M_{n+1}$	$M_1\Omega M_2$	$M_2\Omega M_3$	$M_3\Omega M_4$	$M_4\Omega M_5$	$M_5\Omega M_6$	$M_6\Omega M_1$
	56.5	65	52.5	60	62	62

Table I: Latitude and longitudinal angle values (in degrees) for all 18 star spots on the large Mercedes-star quartz sphere. The grey boxes indicate data that deviate most significantly from their expected values.

Movement of the Stars with Rotation of the Sphere. The sketch in Figure 7 shows how the stars move upon rotation of the sphere in various directions. In all cases in Figure 7, the light source and the observer are perpendicular to the drawing plane. On each circle representing a projection of the sphere, black points show the positions of the star spots, and various manifestations of the three- and four-rayed stars are shown as shaded bands. Two directions of rotation are shown in a series of five steps:

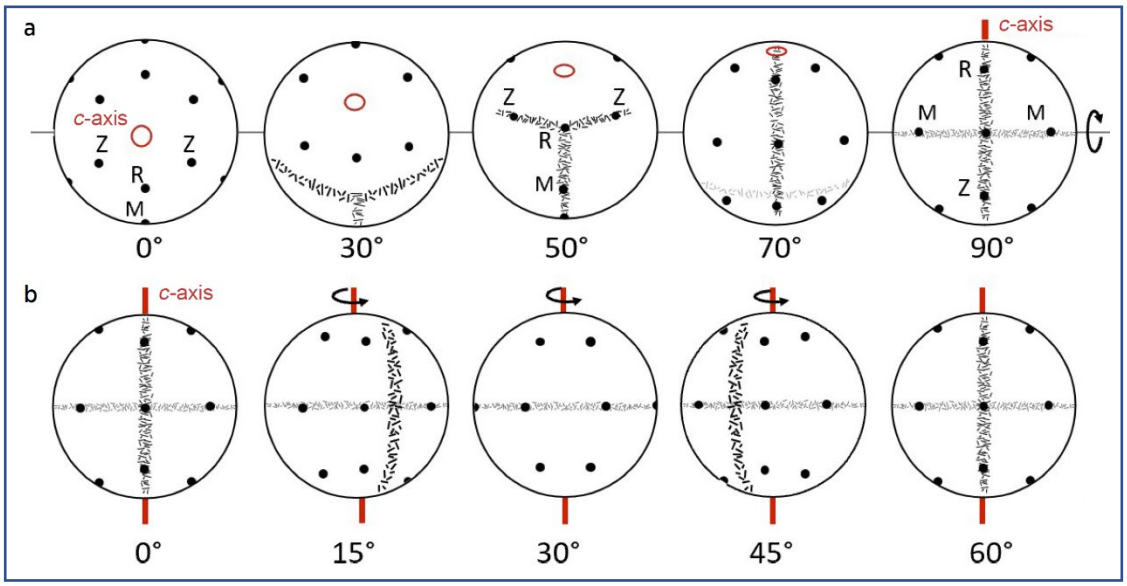

Figure 7: Sketches of the different aspects of the asterism on the large Mercedes-star quartz sphere are shown with the source and observer fixed in the same direction perpendicular to the drawing plane. The black points represent the star spots, and the stippled bands correspond to the branches of the stars. (a) At 0º (far left), the sphere is positioned with the *c*-axis (red circle) of the quartz crystal perpendicular to the drawing plane. Rotation is then carried out around a horizontal axis with angular values of 30°, 50°, 70° and 90° (from left to right). A three-rayed star, absent at 0°, appears near the bottom of the sphere at about 30°, reaches specular reflection at 50° and then disappears near 70°, where a four-rayed star begins to rise up to, at 90°, the centre of the hemisphere. (b) Starting from the last position above, rotation around the vertical three-fold *c*-axis at angular values of 15°, 30°, 45° and 60° (from left to right) show the movement of a four-rayed star.

1. In Figure 7a, the sphere is rotated around a horizontal axis, starting with the *c*-axis perpendicular to the plane of the drawing (parallel to the direction of the light source and the observer). Initially, a set of six star spots forms a virtual hexagon, with no visible optical effect. They move towards the top of the sample as the rotation progresses, and a three-rayed star appears at the bottom after around 30° of rotation. At 50°, the centre of this star is positioned at the centre of the sphere. Further rotation of around 70° causes it to disappear at the top of the specimen, giving way to a cat's-eye-like line occupying the entire height of the sphere. A four-rayed star then appears at the bottom, whose centre eventually occupies the centre of the sphere after a 90° rotation.

2. In Figure 7b, the sphere is rotated counter-clockwise around the vertical *c*-axis, starting from the last position in Figure 7a. The four-rayed star moves away to the right and then disappears, and then another four-rayed star appears from the left.

Additional Stars Visible with Transmitted Light (Diasterism). The distribution of the three-rayed star spots on the egg-shaped sample indicated that its P–P' axis lay along the quartz *c*-axis. Two unexpected (and not previously described) six-rayed stars were observed at each pole of the egg when this somewhat transparent specimen was illuminated from behind with a standard white-light torch parallel to the *c*-axis (Figure 8). To see the six-rayed diasterism, the lamp had to be held a few tens of centimetres from the opposite end of the egg. Bringing the lamp closer to the egg caused the star to disappear. Using the same light source, we did not observe any such six-rayed stars on the sample by reflection at the top nor the base of the egg.

Precessional movement of the lamp around the axis induced movement of the star that was exactly as observed for a rose quartz sphere that displayed similar diasterism (Killingback 2006). When the lamp was moved to the right of the axis, the star moved to the left. However, the star disappeared with further angular deviation of the lamp from the *c*-axis.

When the six-rayed star was centred on the *c*-axis, its branches lay along the same meridians as the Mercedes-star spots (again, see Figure 8). The six-rayed diasterism is also apparently created by illumination of rutile needles, as for the three- and four-rayed stars. However, exact cause of this newly discovered type of star needs further investigation.

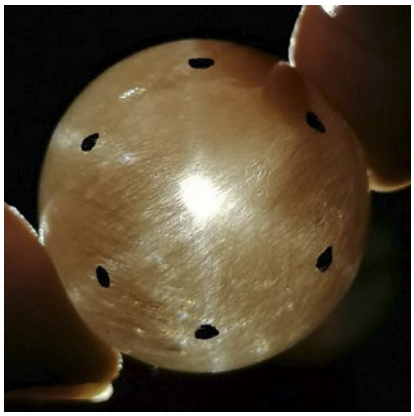

Figure 8: A six-rayed star appears when illuminating the semi-transparent egg-shaped quartz from behind (diasterism), with the light direction parallel to the *c*-axis (perpendicular to the plane of the image, which is also the symmetry axis of the egg). The black points mark the positions of three-rayed star spots. The diameter of the egg's cross-section is 30 mm. Photo by T. N. Bui.

Microscopic Observations

Inclusions. All three quartz samples contained abundant more-or less-curved needles, which we assumed to be typical rutile inclusions. This was confirmed by Raman spectroscopy.

The large sphere shown in Figure 1a appears dark brown, probably due to the large amount of brown rutile inclusions present. The egg-shaped sample is lighter in colour and looks somewhat reddish. Although the host quartz is transparent, the density of the rutile inclusions restricts visibility through the interiors of the stones. The rutile needles have many different

aspects, but most are gently curved and look like 'Venus hairs' (i.e. fine golden to reddish curved needles), scattered randomly in the quartz matrix (Figure 9a). Some straighter ones sometimes cross at a node (Figure 9b). Others are roughly aligned in 'combs' that form two planes joining along a coarser crystal, as in 'platinum quartz' (Koivula & Tannous 2003; Figure 9c), consistent with the tetragonal nature of the central rutile crystal. Interestingly, healed fractures sometimes transect many rutile needles or 'hairs' (Figure 9d). Rutile inclusions can also be accompanied by two-phase fluid inclusions decorating healed fractures (Figure 9e). Because of the random orientation of the rutile needles, one might assume *a priori* that, despite their abundance, they have little to do with the asterism. Nevertheless, due to their high density, the possibility that they could play a role should not be overlooked.

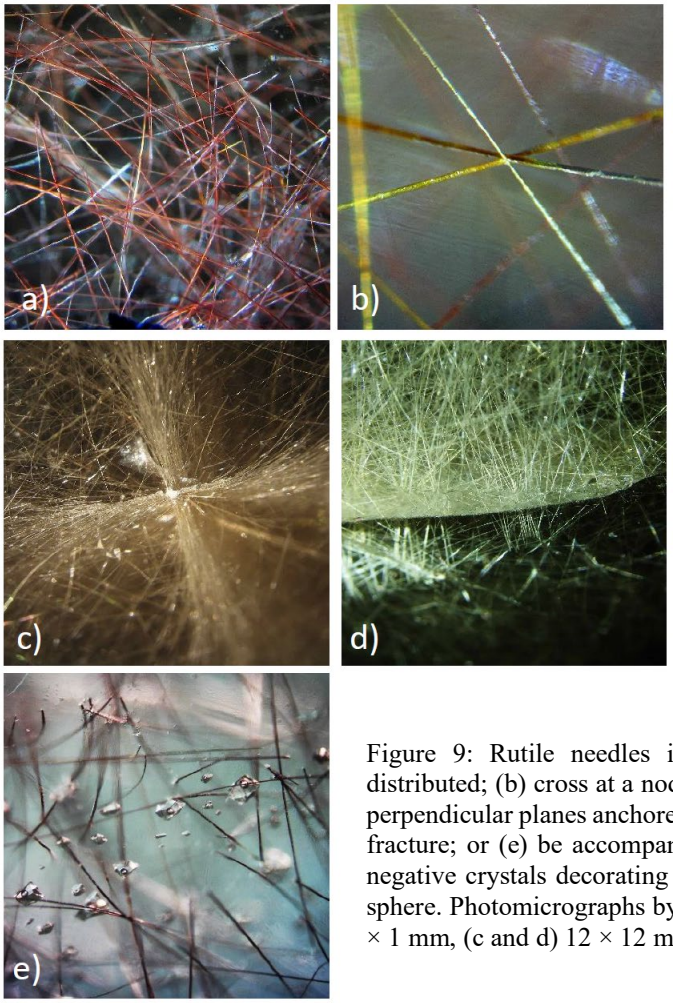

Figure 9: Rutile needles in Mercedes-star quartz can (a) be randomly distributed; (b) cross at a node; (c) have comb-like structures arranged in two perpendicular planes anchored on a larger straight crystal; (d) transect a healed fracture; or (e) be accompanied by two-phase fluid inclusions consisting of negative crystals decorating a healed fracture. All images are from the large sphere. Photomicrographs by J.-P. Gauthier; field of view (a) 3 × 3 mm, (b) 1 × 1 mm, (c and d) 12 × 12 mm and (e) 3 × 3 mm.

Water-Drop Test. The water-drop test is typically performed on flat or even unpolished surfaces to detect chatoyancy or asterism (Gauthier 2011). The test consists of applying a small drop of water on the surface of the stone using a syringe fitted with a hypodermic needle. Observing the sample through the curved surface of the water drop allows one to check for an optical effect due to a possible network of very fine oriented inclusions, invisible under an optical microscope, which could justify classical asterism.

We repeated this experiment on several parts of the large sphere, including on arms and nodes of the stars, and at the ends of the *c*-axis. All of the tests proved negative, ruling out the possibility of a classical scattering phenomenon due to sets of tiny parallel needles.

Reflections from the Rutile Needles. As mentioned above, the branches of the stars do not appear continuous, as for normally chatoyant and asteriated stones. Instead, they consist of concentrations of illuminated segments of randomly oriented acicular rutile inclusions, giving the appearance of the bright reflective dots or lines mentioned above and seen in Figure 10a. The bright lines seem to be due to reflections from the needles' surfaces. The needles act like a multitude of mirrors giving the shiny aspect to the branches of the stars. The needles are not illuminated along their entire length, for at least two reasons: (1) even if the incident rays come

from a parallel beam of light, the rays refracted in different points of the sphere are no longer parallel and arrive in different orientations on a rutile needle, and (2) many of the rutile needles are curved.

The cross-sections of the individual needles are significantly smaller than those found in typical coarse rutilated cat's-eye quartz (Johnson & McClure 1997; Koivula & Tannous 2004). In our samples, the width of these rutile needles, measured on enlarged photomicrographs taken with a binocular microscope at 80× magnification, is about 50 µm and never exceeds 100 µm. The reflections from the needles are actually composed of very thin luminous striae, as seen only at high magnification (Figure 10b).

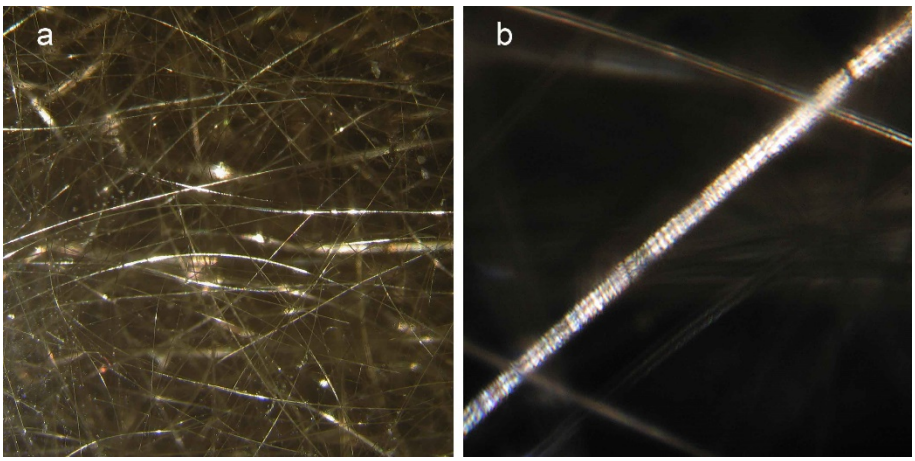

Figure 10: (a) Rutile needles in the large quartz sphere are mainly illuminated in a direction that is roughly parallel to the star branch (here, in a horizontal direction). The orientations of the reflections are best observed by slightly squinting when looking at the picture. (b) At high magnification, the shiny reflective segments of the rutile needles show a striated appearance. Photomicrographs by J.-P. Gauthier; field of view (a) 10 × 10 mm and (b) 1 × 1 mm.

Brewster Fringes in the Quartz. The smaller Mercedes-star quartz sphere was sliced parallel to two planes at 90°: (1) along the equatorial plane perpendicular to the *c*-axis and (2) parallel to the *c*-axis. When the curved surface of a resulting quarter-sphere sample (Figure 11a) was illuminated from above parallel to the *c*-axis, we observed iridescent colours (Figure 11b).

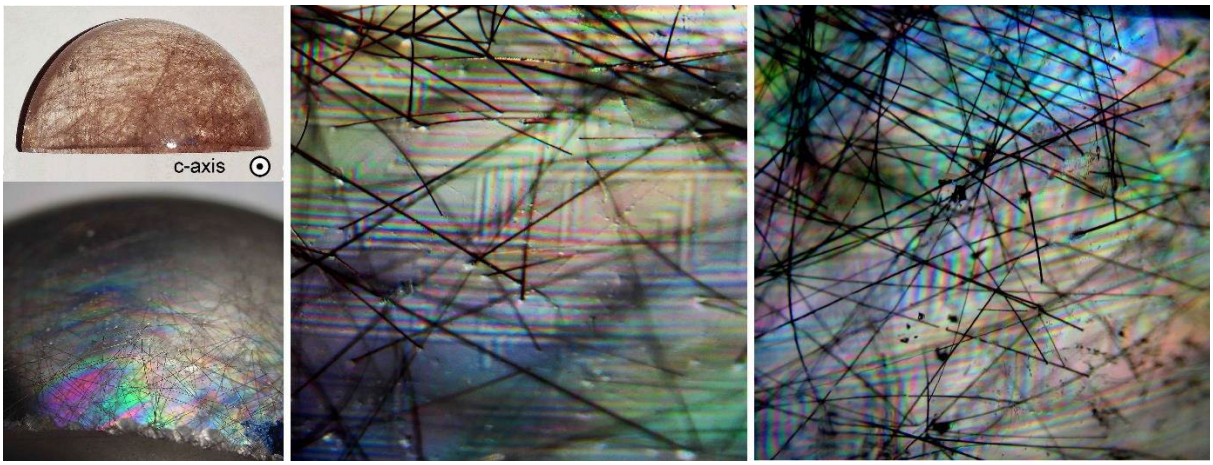

Figure 11: (a) A quarter-slice from the small quartz sphere (28 mm diameter), bounded by two planes at 90°, is shown from above, lying on its equatorial plane with the *c*-axis perpendicular to the plane of the picture. (b) In reflected lighting, it shows iridescent colours. Between crossed polarisers, with illumination from the rear and higher magnification, two distinct sets of Brewster fringes appear with (c) rectangular and (d) parallelogram shapes. Photo(micrograph)s by J.-P. Gauthier; field of view (b) 10 × 10 mm, (c) 3.5 × 3.5 mm and (d) 4 × 4 mm.

With transmitted lighting and crossed polarisers, we observed rectangular or parallelogram-shaped domains underlined by interference colours at different levels within the sample (Figure 11c, d). These features correspond to Brewster fringes, and are due to alternating twin lamellae seen between crossed polarisers, as reported in amethyst (see, e.g., Lu & Sunagawa 1990; Notari *et al.* 2001; Schmetzer 2017). However, they do not have the same sectorial appearance as seen in amethyst. Nevertheless, they reveal the presence of superimposed domains of left-handed and right-handed quartz, corresponding to Brazil-law twinning.

Crystallographically Oriented Thin Sections. To better document the internal structure of the Mercedes-star quartz, two petrographic thin sections (each about 30 µm thick) were cut from the smaller sphere, parallel to the two slices described above. This yielded a full disc parallel to the first slice (S1, oriented perpendicular to the quartz *c*-axis at the equatorial plane) and a half disc cut from one of the remaining hemispheres (S2). Thus, the perimeter of S1 contained six four-rayed star spots, and the hemispherical circular edge of S2 contained two three-rayed and two four-rayed star spots, as well as the *c*-axis (Figure 12a).

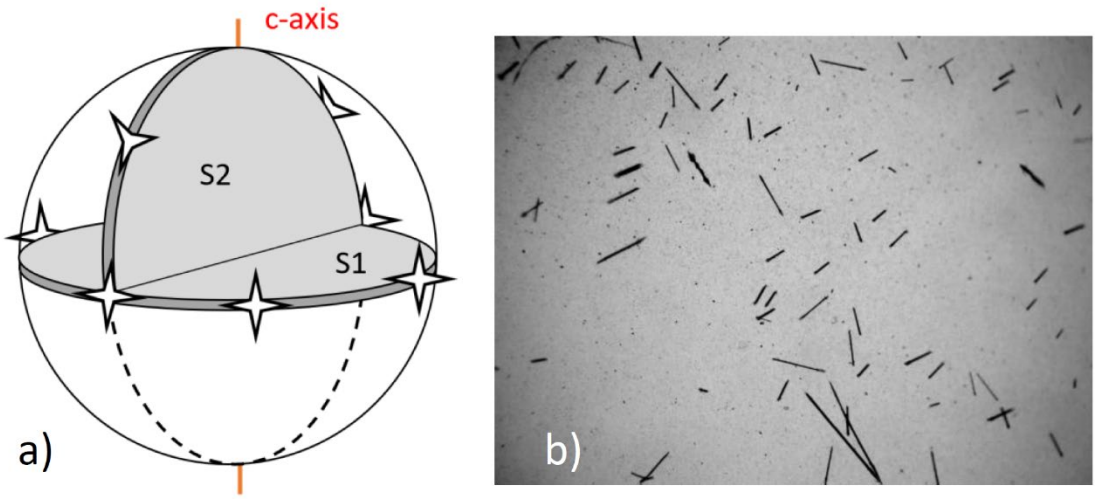

Figure 12: (a) A diagram shows the orientation of two slices cut from the small Mercedes-star quartz sphere, with star spots schematically represented along their rims. Slice S1 was cut perpendicular to the *c*-axis along a plane containing six four-rayed star spots. Slice S2 was cut perpendicular to S1 along a meridian containing two three-rayed star spots and two four-rayed star spots. (b) The general aspect of these slices, seen illuminated from behind and without light polarisation, shows only randomly oriented segments of rutile needles (here, in slice S1). Photomicrograph by J.-P. Gauthier; field of view 4 × 3 mm.

With transmitted light, and without polarisers, no remarkable features stood out within the quartz matrix, except for randomly oriented segments of rutile needles (Figure 12b). By rotating the slices between crossed polarisers, both samples became uniformly dark. Then, when rotating the analyser about 1° further, a checkerboard pattern with dark and bright tiles appeared (Figure 13). The pattern reversed when the analyser was rotated in the other direction. This behaviour is expected for Brazil-law twin structure made up of right- and left-handed quartz.

This process is further illustrated using the slice cut parallel to the quartz *c*-axis (S2). In Figure 14a, the polariser is initially parallel to the base of the half-disc (that is, perpendicular to the *c*-axis). The crossed polarisers are then rotated until the sample shows extinction (Figure 14b). Finally, a slight rotation of the analyser reveals the tiles and twin boundaries (Figure 14c), which are oriented at around 50° from the horizontal. This is very close to the inclination of the *r* or *z* planes of the rhombohedron (i.e. 51°27′; Frondel 1962, p. 340).

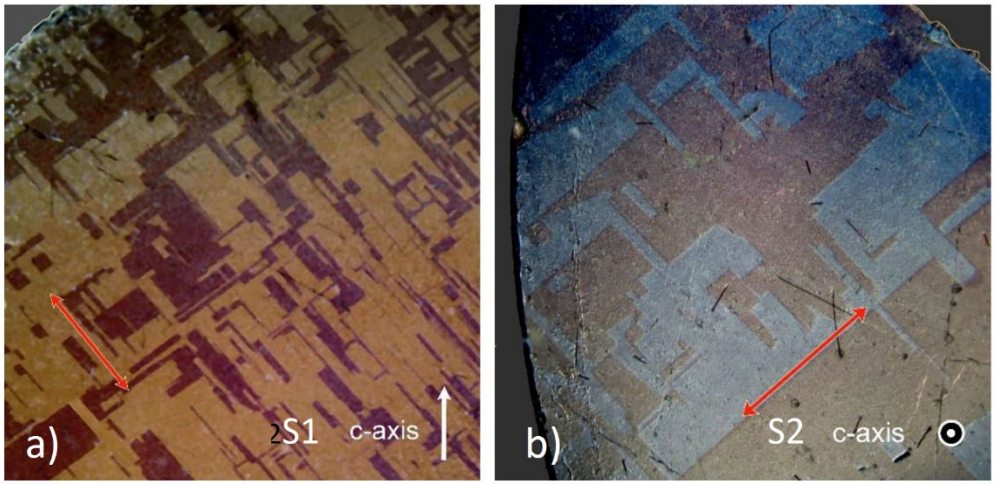

Figure 13: Viewed between crossed polarisers, a slight rotation of the analyser from the extinction position reveals tiling quartz slices S2 (a) and S1 (b) that is typical of Brazil-law twin structure made up of right- and left-handed quartz. Contrast was enhanced to make the structures more distinct. The double red arrow indicates the position of the analyser at extinction. Photomicrographs by J.-P. Gauthier; field of view (a) 10 × 10 mm and (b) 5 × 5 mm.

Unfortunately, there is no crystallographic reference for the horizontal slice (S1). We simply note that extinction occurs when the analyser is parallel to the twin edge (Figure 13b).

It is interesting to note that the tilt angle of the normal (with respect to the horizontal) to the twin boundaries is approximately 40° (again, see Figure 14c), which is also the latitude of the three-rayed star spots (see Table I).

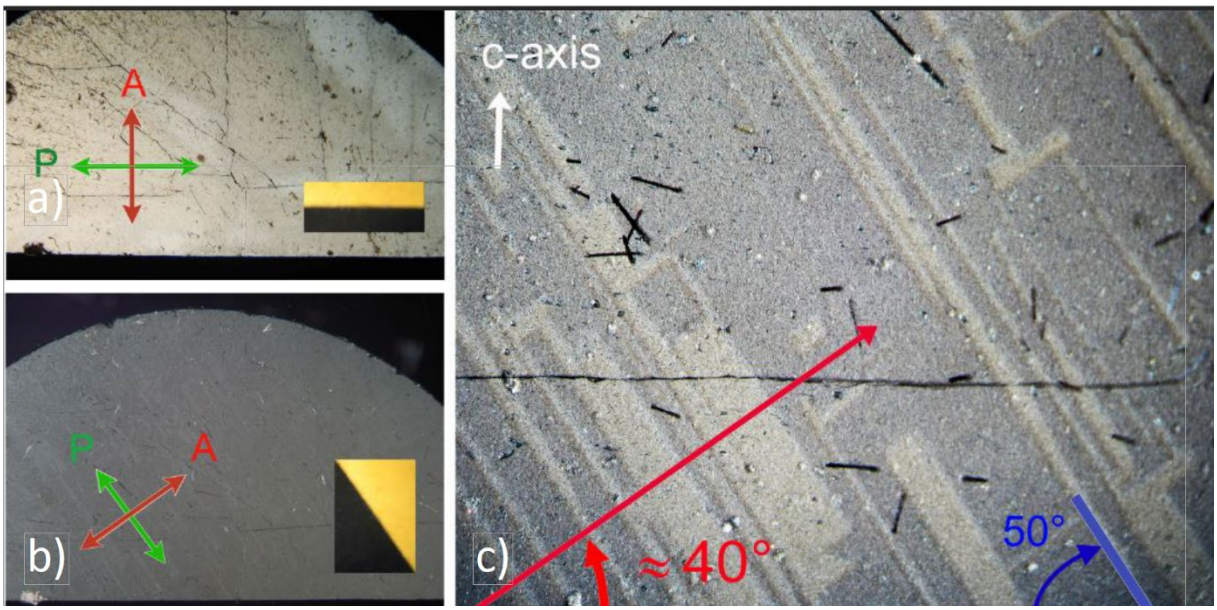

Figure 14: Observation between crossed polarisers of quartz slice S2 reveals: (a) when the polariser axis (P) is first aligned with the horizontal diameter (28 mm) of the half disc, the area appears bright, but (b) by turning the crossed polarisers about 50°, the area becomes almost uniformly dark. (c) By further rotating the analyser (A) by a few degrees, a tiled geometric structure becomes visible. The elongated direction of the structural elements is parallel to the direction of the polariser in Figure 14b. The 40° angle between the red arrow (analyser) and the horizontal corresponds to the latitude of the three-rayed star spots (see Table I), as well as the normal to the rhombohedral faces. (The yellow self-adhesive birefringent tape in (a) and (b) shows the rotation angle of the polariser.) The red arrow indicates the position of the analyser. Photomicrographs by J.-P. Gauthier; field of view 3.5 × 2.65 mm for image c.

DISCUSSION

Proposed Mechanisms of Asterism in Mercedes-Star Quartz

Since we have excluded the presence of sets of invisible parallel fibres leading to a scattering effect, and because randomly oriented rutile needles alone cannot explain a directional optical effect, we must consider a more complex mechanism for the network of stars seen in Mercedes-star quartz, involving both of the following elements highlighted by the experimental observations:

1. The presence of Brazil-law twin planes, as revealed both by Brewster fringes and by tiling inside the samples. Not directly visible without polarisers, these can act as reflecting planes due to the change in chirality of the quartz (from left to right, for example), resulting in a slight change in refractive index at the interface.

2. The illumination of some needles, thus playing an obvious role in the formation of the star branches. As the bright reflective markers of the branches, we presume they operate in a second step to produce the asterism.

Figure 15a shows a set of parallel Brazil-law twins (in white) acting as mirrors, and a meridian plane that is perpendicular to this set. With the light source and observer positioned above the quartz sphere, any vertical ray (blue or red) entering this meridian plane will be reflected, by any twin of this set, within this meridian plane. Now consider another set of randomly oriented reflecting planes, none other than the mirror planes observed on rutile needles. The preceding blue and red rays can only be reflected back to the observer by the planes of the rutile needles whose normal lies in the meridian plane (optical paths in blue and red). In any other situation—such as for rutile reflecting planes whose normal is not in the meridian plane, or for incident rays entering outside the meridian plane—the twice-reflected rays usually will not reach the observer.

These conditions are very restrictive, but all rays reaching the observer must cross the sphere on the rim of a meridian plane, giving rise to a luminous branch corresponding to multiple small planes of reflection.

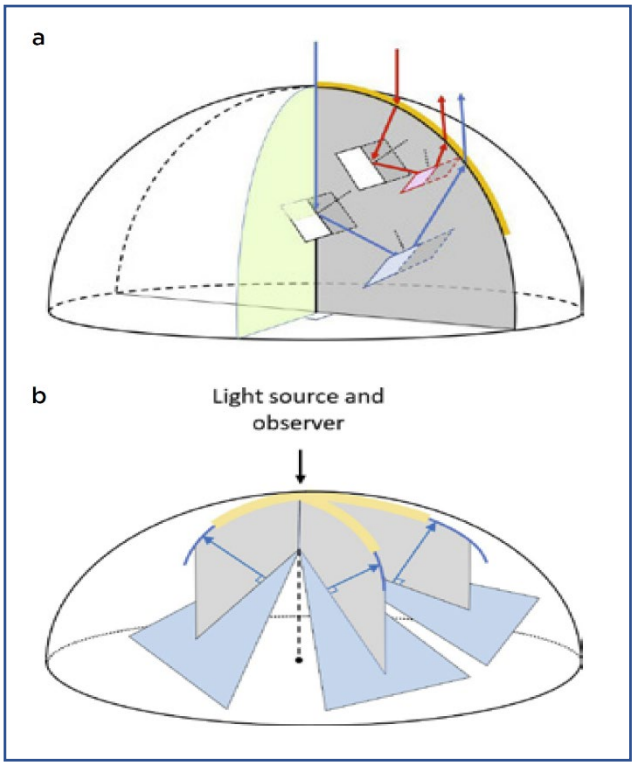

Figure 15: (a) This diagram shows the optical path of light rays propagating in a meridian plane that is perpendicular to a set of twin planes (white) in Mercedes-star quartz. A second reflection on a plane (blue or red; belonging to a rutile needle) perpendicular to the meridian plane is necessary for the rays to reach the observer (red or blue paths). The set of rays propagating in (or close to) the meridian plane toward the observer gives rise to a branch of a star (in yellow). (b) A general model is depicted for producing a three-rayed star (in yellow) due to the reflection of light from three sets of mirrors (in blue) and then from small planes belonging to the needles (not shown here). The branches of the star lie along three great circles (meridian planes in grey) containing the incident beam and the normals (blue arrows) to the reflecting planes. In Mercedes-star quartz, the three-rayed stars are not seen along the three-fold axis, but they are visible at an angle of about 50° from it.

Figure 15b shows, diagrammatically, three sets of primary reflectors (blue), which are required to produce a three-rayed star (yellow) on the rim of the three meridian planes (grey) associated with these stars.

So that the branches do not extend beyond the top of the hemisphere—otherwise a six-rayed star would result from the three sets of reflectors—there must be no reflector plane behind the plane perpendicular to the meridian plane, shown in green on Figure 15a. We discuss later if this condition may be satisfied.

Which Planes Are Involved? For the large quartz sphere studied here, the only crystallographic information is the position of the *c*-axis. However, three sets of reflecting planes are needed that are suitable to explain the observed three-rayed stars, (again, see Figure 15b) and four planes for four-rayed stars. It is worth remembering that the three-rayed stars are not viewed down a three-fold axis (*c*-axis) of the quartz.

Brazilian quartz (as well as quartz from other sources) is known to exhibit 'Brazil twins', also known as chiral or optical twins (see, e.g., Schmetzer 1987; Lin & Heaney 2017). This is one of two categories of twins with parallel axes known in quartz that is involved here, as shown by the observations between crossed polarisers (Figures 13 and 14). The faces of the twinned volumes shown in Figure 16a are crystallographic planes belonging to the first-order prism *m* {10$\underline{1}$0}, positive rhombohedron *r* {10$\underline{1}$1}, negative rhombohedron *z* {01$\underline{1}$1} (see Figure 16b), basal plane *c* {0001} and triangular dipyramid *s* {11$\underline{2}$1}. Very often, they are manifested in the form of thin, repetitive plates (polysynthetic twins parallel to *r* or *z* planes; Frondel 1962, p. 387). In particular, the lamellar structures in Figure 16c strongly resemble those described by Sunagawa *et al.* (2009) showing the parallelograms that are seen in Brewster fringes.

The most frequently encountered and largest crystallographic planes in quartz usually correspond to the faces of the rhombohedra *r* and *z* and the first-order prism *m*. These are, therefore, the planes that we preferably choose to explain the Mercedes-star quartz asterism. This choice is not made at random. Indeed, as mentioned above, in quartz the angle between the rhombohedral planes *r* or *z* and the basal plane *c* is 51°47′, very close to the angular position of the three-rayed star spots relative to the poles, north or south, at about 50° (Table I).

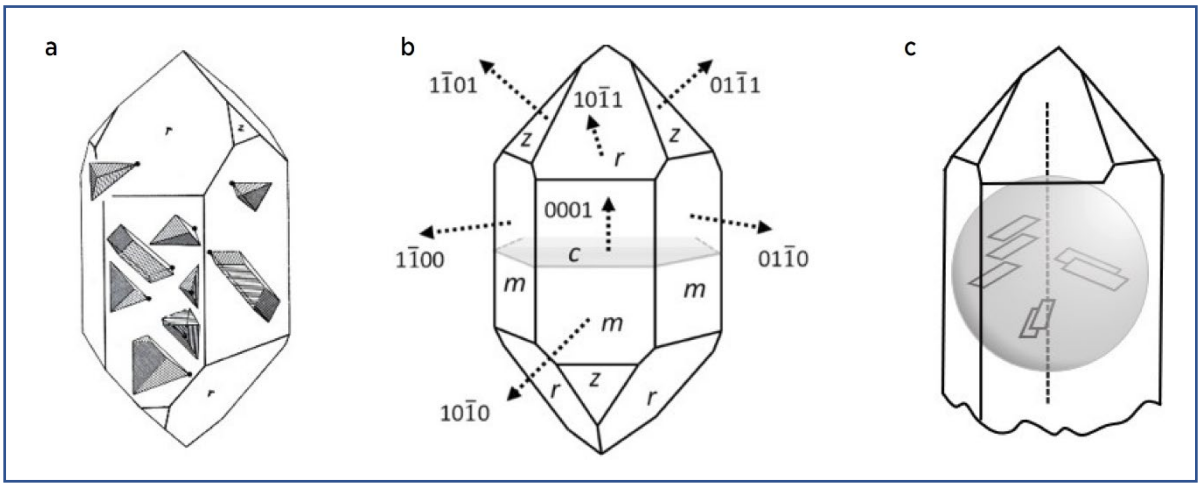

Figure 16: (a) This sketch illustrates Brazil twin domains inside a quartz crystal, after Frondel (1962, p. 387). (b) A crystal model displays the main faces that develop on quartz and their normals. Similar twin planes lie within the crystal. (c) When 'cutting' a sphere from single-crystal Mercedes-star quartz, it is assumed that the Brazil twin planes do not to extend beyond the central axis.

In addition, it has been assumed that each set of reflecting planes lies on only one side of the vertical sphere diameter (as shown in Figures 15 and 16c) to explain the fact that the branches end at the star centre. It is not possible to have an equivalent reflecting plane (either rhombohedral or prismatic) on the other side of the *c*-axis, simply because it is not also a binary (two-fold) axis. So the plane on the other side is necessarily of a different nature, and thus cannot reflect light the same way. Also, it is probable that within a quartz prism, a sphere will be cut by the lapidary that is centred within the crystal, if only to obtain the maximum yield (Figure 16c).

Demonstrating the Involvement of These Planes. Consider the observations between the rotation angles 0° and 50° shown in Figure 7a. In the first case, the observer and the light source are in the direction of the quartz's three-fold axis (the *c*-axis). The observer does not see any optical effect. By rotating the sphere upwards by 50° around the horizontal axis in the plane of the drawing, a three-rayed star appears, with a light beam entering perpendicular to the surface of the sphere, thus not deflected by refraction.

According to the above, the branches of the star will follow the meridians associated with three great circles containing the incoming beam and each of the normals to the reflecting planes. It is then necessary to see if, after rotation by 50°, the chosen planes can justify the appearance of the branches of the three-rayed star in the observed directions.

Stereonet for Three-Rayed Stars. Stereographic projection (e.g. Figure 17) is a method of projecting points and angles onto a circle on a two-dimensional diagram called a stereonet (also known as a Wulff diagram; Bloss 1971; Shelley 1985; see Box A). For this discussion, the light source and the observer are always directed along the vertical axis of the projected sphere (i.e. perpendicular to the plane of Figure 17). We assume that the quartz *c*-axis <0001> initially coincides with this direction, represented by the centre of the stereonet. The other three axes of the quartz are labelled a_1, a_2 and a_3 along the edges of the projection disc (the a_3 axis is omitted from Figure 17 for clarity).

Figure 16b shows the crystal faces that are most likely be present within a quartz crystal as reflecting twin planes. These are the *r* and *z* rhombohedral faces and *m* faces of the first-order prism. With respect to the *c*-axis, the normals to the faces projected on the stereonet in Figure 17a—from left to right, *z* (1$\underline{1}$01), *r* (10$\underline{1}$1) and *z* (01$\underline{1}$1)—make an angle of about 51°47′ with respect to the *c*-axis (Frondel 1962, p. 340), and are, before the rotation, on the same projection circle as the red points in Figure 17a. The projection of the first-order prism face *m* (10$\underline{1}$0) is also labelled in red at the edge of the stereonet.[1] The situation in Figure 17a is similar to that of Figure 7a for the 0° angle, where the black points represent the star spots.

Starting from this configuration, rotation of the quartz sphere around its a_2-axis from bottom to top by 50° is equivalent to the 50° position in Figure 7a. Then, the poles (initial positions in red in Figure 17) of the *r* and *z* faces move along 'parallels' of the stereographic projection (red arrows on Figure 17a), along which it is possible to count 50° and fix their new positions. We see that the pole *r* (in green) is then at the centre of the stereographic projection in Figure 17a (i.e. facing the direction of the incident light beam), and that the segments joining it to the two poles *z* make an angle of about 130°. This is exactly the situation in Figures 3c and 7a (centre), where the star spot of a three-rayed star is at the centre (position of green *r*) and the

[1] With rotation of 60° around the *c*-axis of the quartz, an analogous situation would occur first with faces *r*, *m*, *r*, and then with the *m* face of the first-order prism. Therefore, if the three-ray star spot at A1 (longitude 0° for instance) in Figure 5a is produced by a set of *z*-*m*-*z* faces, the next star spot A2 (thus at the longitude 60°) will be produced by a set of *r*-*m*-*r* faces. Thus, the use of stereographic projection is valid for each three-rayed star.

Box A: Stereographic Projection on a Stereonet

This box focuses on angular displacements of the normals to the twin planes when a quartz sphere is rotated around an axis. Stereographic projection can help follow the paths of the ends of normals that originate at the centre Ω of a virtual sphere, with their ends Q on the external surface of this sphere (assumed to have a very large diameter compared to the size of a quartz crystal). As described below, the south pole P' of the sphere plays a special role for points in the northern hemisphere (and by analogy, the north pole P has a similar role for points in the southern hemisphere, making it possible to confine all projections inside the stereographic circle).

By definition, the stereographic projection of the end N of any normal Ω–N of the northern hemisphere is located at point Q, which is at the intersection of the equatorial plane and the line joining N to the south pole P' of the sphere (Figure A-1). In Figure A-1a, if we consider all the points N on the circle (C) perpendicular to the west-east direction (W–E), characterised by an angle NΩE = α, their stereographic projection is represented in the equatorial plane by the curved red line Q–Q'. Note that the stereographic projection of a great circle (C') is projected as a line following the diameter of the equatorial plane.

In Figure A-1b, for a point N on a great circle (D) passing through the diameter W–E and tilted by β with respect to the horizontal plane, its stereographic projection Q is located on a curved green line, joining W to E.

On the stereonet (Figure A-1c), the two types of lines (green and red) corresponding respectively to α and β (represented by blue segments showing angles α = 50° and β = 20°) are shown on a circle gridded at 10° intervals (more detailed stereonets are gridded at 2°, as in Figure 17 in the text). As an example, if Q' is the projection of N' obtained after rotation from ΩN to ΩN', each projection line provides the corresponding values of the angular deviations δ between ΩN and ΩN' (i.e. rotation of δ = 80° shown in red and green, respectively, in Figure A-1c). The network of curves in a stereonet makes it straightforward to follow the displacement of the normals to the growth planes or twin planes as a sample is rotated.

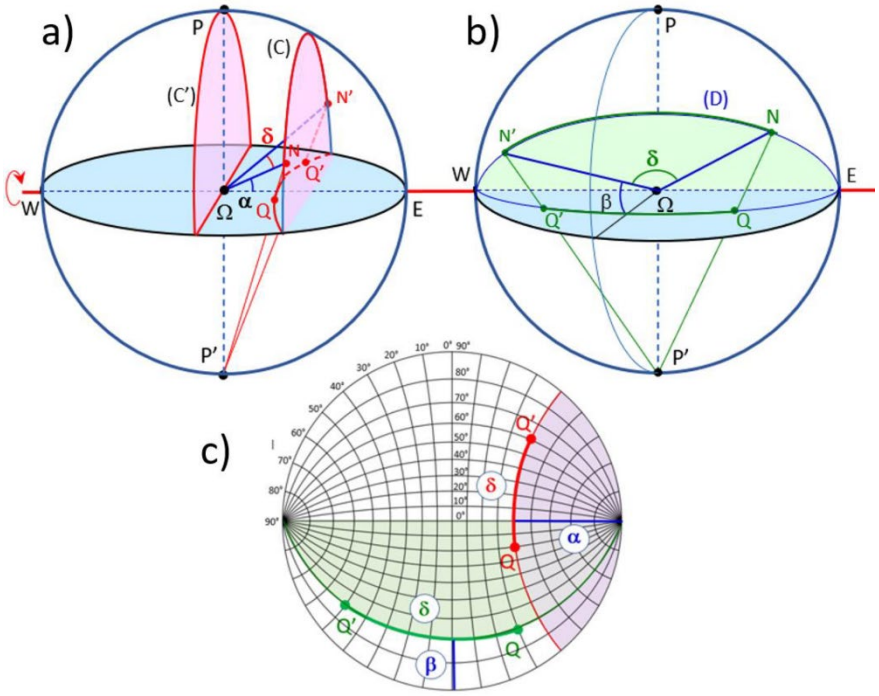

Figure A-1: Stereographic projection can be used to evaluate the angle δ between two normals ΩN and ΩN'. Their ends N and N' are located (a) on a circle (C) perpendicular to the W–E axis, or (b) on a great circle (D) containing this axis. (c) The stereographic projections Q and Q' of N and N' are located on the same line (red or green) plotted on the stereonet, making it possible to measure the angular deviation α and β. In this example, the projection of circles (C) and (D) illustrates the angles they make with the horizontal plane (α = 50° and β = 20°, respectively, represented by blue segments). The angular deviation between ΩN and ΩN' is δ = 80°, counted on the red or green line.

star branches are located on three great circles containing the incident beam and each of the normals to the reflecting planes. The intersection of these three great circles corresponds to the normal to the *r* plane. Note also that the angle of 130° between the branches is not distorted by the stereographic projection, which allows measurement of the real angles on a photograph taken perpendicular to the sphere surface at the centre of a star (again, see Figure 3c).

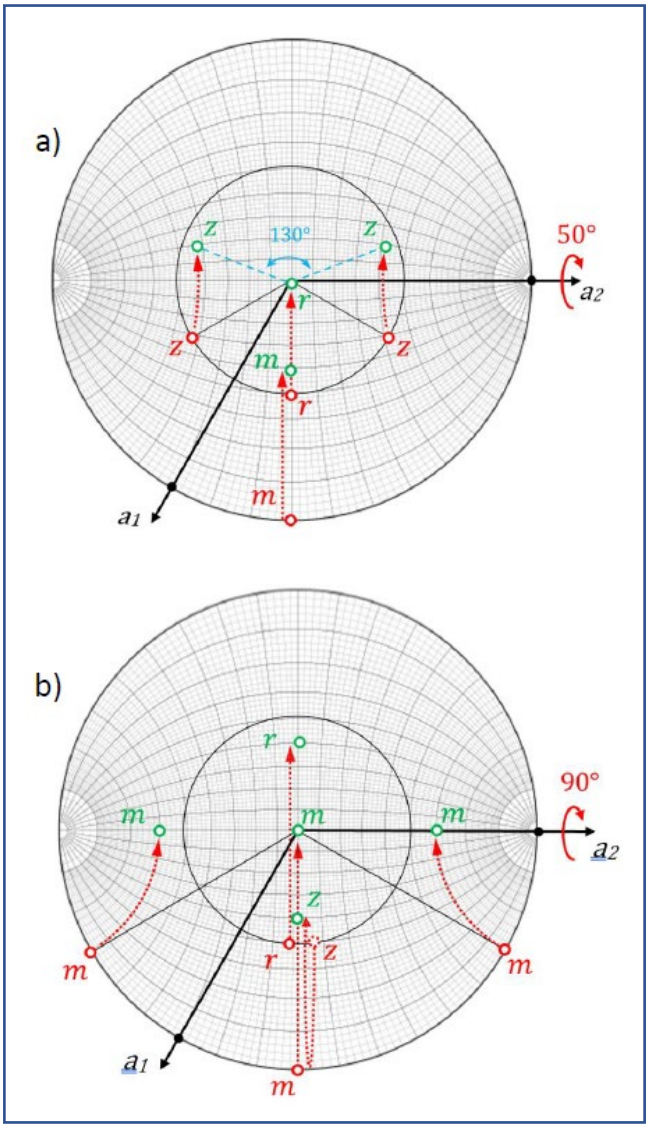

Figure 17: In order to show the correlation between star spots and twin plane directions in Mercedes-star quartz, these stereonets show the movement of the *m*, *r* and *z* poles of a quartz crystal when rotated about the a_2-axis, from an initial position (in red) such as that drawn in Figure 7a (at 0°). (a) A 50° rotation brings the poles of faces *m* and *z* (in green) into the same position as shown in Figure 7a (at 50°) with pole *r* at the centre of the diagram (i.e. in the direction of the light source and observer, and coinciding with the centre of the three-rayed star). (b) Similarly, a 90° rotation brings pole *m* into the centre of the diagram, coinciding with the centre of a four-rayed star in Figure 7a (at 90°). Arrows indicate the movement of the different poles.

Given the experimental errors, we propose that the approximate measured value of 50° for the angular positions of the three-rayed stars (points A_n and B_n in Figure 5b) with respect to the north (P) and south (P') poles fits the theoretical angular value of 51°47′ of the *r* and *z* faces of the rhombohedra with respect to the horizontal (Frondel 1962, p. 340). Importantly, we have shown that the normal to one face of the rhombohedron is coincident to the direction of the light beam, when looking at the star spots. Similarly, the angular value of about 50° measured between crossed polarisers on the twin planes with respect to the horizontal in Figure 14c is close to the experimental value corresponding to the tilt of the rhombohedral faces.

This demonstrates that our measurements are consistent with light reflection on the twinned rhombohedral and prism faces, a rare phenomenon that we propose is responsible for the three-rayed stars through secondary reflections by appropriately oriented portions of the rutile needles.

Stereonet for Four-Rayed Stars. Now consider rotation around the a_2-axis by 90° instead of 50°—that is, from the 0° to 90° position in Figure 7a. The pole of the front first-order prism *m* moves to the centre of the stereographic projection (Figure 17b), and the corresponding plane becomes perpendicular to the incident beam (like the *r* plane in the previous configuration). The poles *m* of lateral planes of the first-order prism migrate on the horizontal axis along the

parallels (red arrows). The pole of face *r* is replaced by that of the lower face *z* (initially in the same position on the stereographic projection, but in the south hemisphere, represented by a dotted red arc), and becomes symmetrical to it with respect to the horizontal axis.

The normals to the four planes around the centre (*r*, *z*, *m* and *m*) are on great circles passing through the direction of the incident beam (centre of the stereographic projection). Thus, the four-rayed stars are due to reflection on two non-adjacent *m* faces and a couple of *r* and *z* faces, followed by secondary reflections from the rutile needles. Regarding the weak intensity of the horizontal branch, we assume, without being able to prove it, that the prism faces of the twin interfaces are poorly developed in (or perhaps absent from) the earlier-described Mercedes-star quartz specimens, and constitute only the edges of the twin lamellae.

Finally, the stereonets in Figure 17 show the strong correlation of star spot positions on Figure 7a (at positions 0°, 50° and 90°) with the normals to the *m*, *r* and *z* twin planes.

Reflection of Light by Rutile Needles

To the naked eye, the needles considered in the proposed mechanism appear to shine continuously. At higher magnification, the illumination of the rutile needles appears as segments of closely spaced bright striae. The brightness of the rutile segments is due to the reflection of light on planar features that are perpendicular or oblique to the axis of a needle (Figure 18). This effect can be emphasized by illuminating the inclusions with a laser pointer (Figure 19).

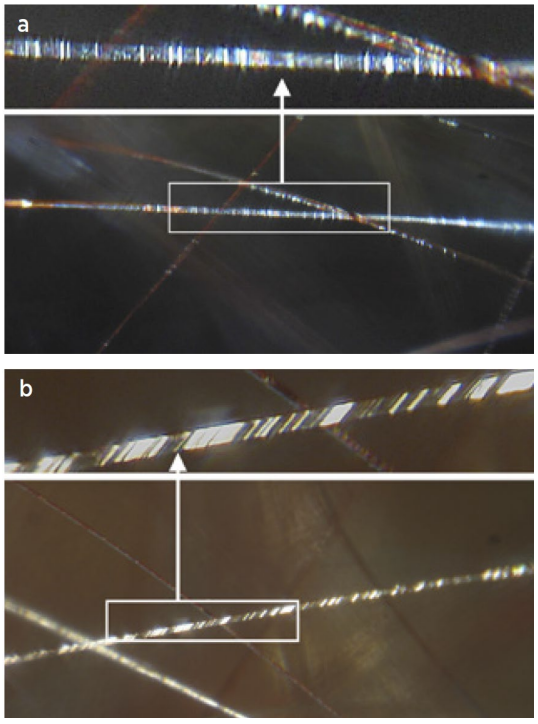

Figure 18: The reflections from the rutile needles consist of striae that are numerous and close together. Depending on the orientation of the needles relative to the light source, they are striated (a) almost parallel to the cross-section or (b) tilted at an angle. Photomicrographs by J.-P. Gauthier; image widths 1.66 mm (a) and 1.89 mm (b), and 0.67 mm for both insets.

Even at high magnification, it is difficult to identify the nature of the tiny reflecting planes on the needles. Are they small facets on the surfaces of the needles, glide planes or planar defects? The answer would require further investigation beyond the scope of this article. For now, it is sufficient to say that these features contribute, as reflectors, to the asterism in Mercedes-star quartz.

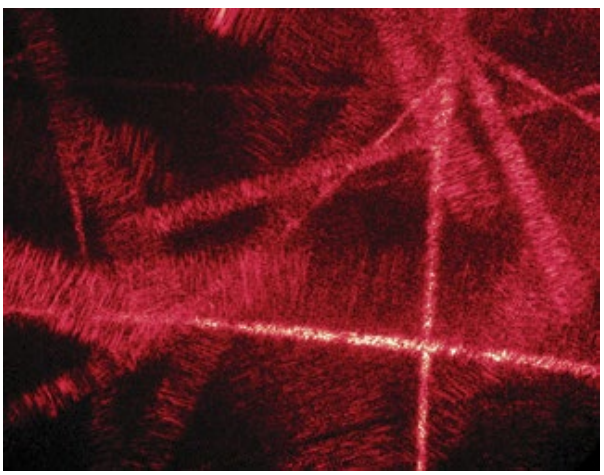

Figure 19: Illumination of the rutile needles with a laser pointer emphasizes their reflectivity. Photomicrograph by J.-P. Gauthier; image width 2 mm.

Very often, the axis of a needle lies in the direction of the light source (Figure 20) and along a branch of the star. When that happens, the reflections of the striae appear to be perpendicular to the needle axis (Figure 18a). Otherwise, the reflections are oblique (Figure 18b) when a needle axis deviates from the orientation of the ligh t source.

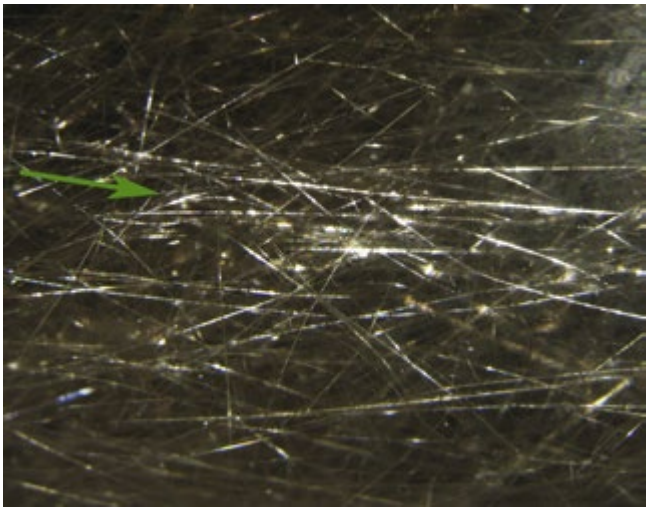

Figure 20: The many illuminated rutile needles in this sub-horizontal star branch are oriented roughly in the same direction (see green arrow). In this case, the mirror striations lie perpendicular to the needle axis, as in Figure 18a. Needles that deviate from the general direction indicated by the arrow correspond to the case of Figure 18b. The sample is illuminated from the top of the photo, approximately perpendicular to the arrow. Photomicrograph by J.-P. Gauthier; field of view 2.5 × 1.85 mm.

The same kind of striae were seen with transmitted light on the needles in the egg-shaped quartz. Without further analysis, we suspect a similar cause for the diasterism in that specimen, this time involving both *r* and *z* faces, with light directed along the quartz *c*-axis.

In summary, the asterism in Mercedes-star quartz is due to a rare combination of properties. In addition to the characteristics of the rutile needles, the host quartz must be finely Brazil-law twinned, with twinned sectors exhibiting rhombohedral and prism faces. Figure 21 shows the faces involved in the first reflection from the twins, for three-and four-rayed stars. In Figure 21a, the normal to face *r* (in grey) is in the direction of a three-rayed star spot, and the corresponding star branches are produced by the primary reflections of twin planes *z*, *z* and *m* (in orange). In Figure 21b, the face *m* (in grey) is in the direction of a four-rayed star spot, whose branches are produced by the lateral *m* planes and by the upper and lower planes *r* and *z*, respectively (in orange). If the quartz is rotated by 60°, the same observation will be made for the two types of stars, simply by inverting the *r* and *z* notations.

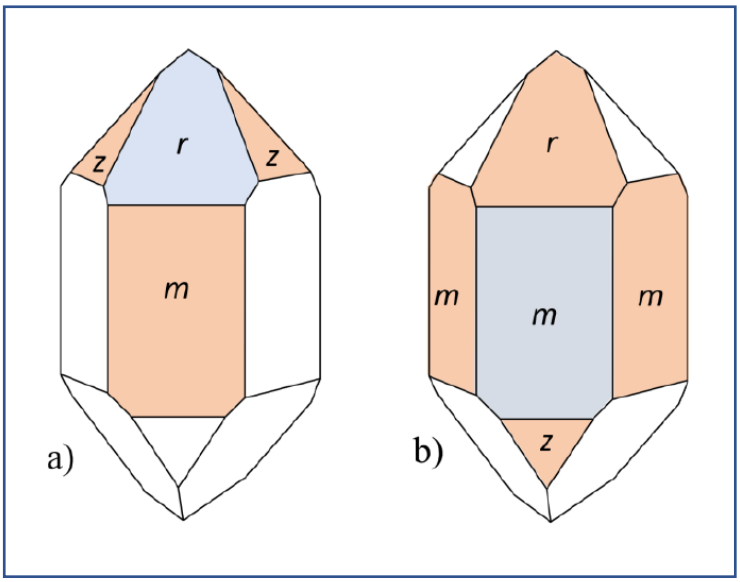

Figure 21: Twin planes participating in the first reflection needed to produce (a) three-rayed stars and (b) four-rayed stars are shaded orange. When a three- or four-rayed star centre is positioned at a star spot, the respective grey planes are perpendicular to the incident beam of light.

CONCLUSION

The unusual asterism observed in Mercedes-star quartz seems to exist only with the simultaneous presence of Brazil-law twins and rutile needles. We therefore propose a plausible mechanism that we can at least partially validate through crystallographic observation and reasoning. This unusual asterism arises from a double-reflection mechanism based on the following observations:

- Classical chatoyancy—light scattering on sets of oriented acicular inclusions—was ruled out due to the absence of parallel needles (even at sub-microscopic scale, as validated using the water-drop test) and by the fact that the branches stop at the centre of each three-rayed star.
- The existence of 'optical twins' in Mercedes-star quartz was visible in slices and in thin sections cut from one of the samples through the presence of Brewster fringes and tiling (Figures 11 and 13). The occurrence of these twins induces the presence of flat reflective surfaces due the change of chirality at the interface between the twin planes.
- This type of asterism has never been documented in transparent quartz containing Brazil twins but without rutile needles. Thus, the needles play a key role in this phenomenon.
- While light scattering on oriented acicular inclusions induces a six-rayed star in minerals with a three-fold symmetry axis, the present phenomenon first requires three sets of reflective planes not related to three-fold symmetry, but which are due instead to Brazil twins.
- Randomly oriented rutile needles can intercept the light reflected from the twin planes and send it back toward the observer, provided that the entire light path is in or near a meridian plane of the quartz sphere. The secondary reflection inducing the asterism is not due to the total surface area of rutile needles, but from numerous, discrete, parallel small reflective elements of the needles, the exact nature of which we could not identify by optical microscopy.
- The locations of star spots, supported by stereographic projections, showed a strong correlation with the directions of the normals to the *r*, *z* and *m* planes.
- Due to the random angular distribution of the rutile needles and, thus, of their reflective elements, a high needle density is required to produce enough reflections toward the observer to create the epiasterism in Mercedes-star quartz. However, when very high inclusion density makes the stone opaque, diasterism cannot be observed.

This study represents a major step towards the understanding of Mercedes (three-rayed) stars in quartz. This relatively rare and particularly complex optical phenomenon is not only related to inclusions, but also to the twinned nature of otherwise transparent quartz. The requirement of both a sufficient density of inclusions and Brazil twins means that specimens are generally large (i.e. multi-centimetre sized). Although less attractive than the usual asteriated gems due to the diffuse appearance of the stars, Mercedes-star quartz is certainly an interesting curiosity for collectors.

REFERENCES

Bloss, F.D. 1971. Crystal projections. *In*: *Crystallography and Crystal Chemistry*. Holt, Rinehart and Winston Inc., New York, New York, USA, 70–298.

Choudhary, G. & Vyas, M.B. 2009. 'Multiphenomenal' quartz from India. *Gems&Jewellery*, **18**(1), 10–12.

Frondel, C. 1962. *Dana's System of Mineralogy, Vol. 3: Silica Minerals*, 7th edn. J. Wiley, New York, New York, USA, xii + 334 pp.

Gauthier, J.-P. 2011. Amusantes et instructives variations sur le thème de la détection de la chatoyance. *Revue de Gemmologie A.F.G.*, No. 178, 21–24.

Gübelin, E.J. & Koivula, J.I. 2005. *Photoatlas of Inclusions in Gemstones*, Vol. 2. Opinio Publishers, Basel, Switzerland, 829 pp.

Gübelin, E.J., Weibel, M. & Wuthrich, A. 1982. Elucidating the optical theory of asterism. *Journal of the Gemmological Society of Japan*, **9**(1), 18–21, https://doi.org/10.14915/gsjapan.9.1_18.

Hainschwang, T. 2007. Gem News International: An unusual type of phenomenal quartz. *Gems & Gemology*, **43**(3), 261–262.

Hyršl, J. & Niedermayr, G. 2003. *Magic World: Inclusions in Quartz*. Bode Verlag, Haltern, Germany, 240 pp.

Johnson, M.L. & McClure, S.F. 1997. Gem Trade Lab Notes: Quartz, cat's-eye effect caused by large rutile needles. *Gems & Gemology*, **33**(1), 59.

Johnson, M.L. & Koivula, J.I. (eds) 1999. Gem News: Twelve-rayed star quartz from Sri Lanka. *Gems & Gemology*, **35**(1), 54–55.

Kane, R. 1985. Gem Trade Lab Notes: Quartz, very dark reddish gray cat's-eye. *Gems & Gemology*, **21**(2), 112–113.

Killingback, H. 2006. Diasterism in rose quartz. *Gems&Jewellery*, **15**(3), 64.

Killingback, H. 2008. The positions of light spots on rose quartz star spheres. *Gems & Gemology*, **31**(1–2), 40–42, https://doi.org/10.15506/jog.2008.31.1.40.

Koivula, J.I. 1987. Gem News: Phenomenal quartz from Brazil. *Gems & Gemology*, **23**(3), 175–176.

Koivula, J.I. & Tannous, M. 2003. Gem News International: "Platinum quartz". *Gems & Gemology*, **39**(4), 334–335.

Koivula, J.I. & Tannous, M. 2004. Lab Notes: Three rutilated quartz cat's-eyes. *Gems & Gemology*, **40**(1), 63.

Lin, X. & Heaney, P.J. 2017. Causes of iridescence in natural quartz. *Gems & Gemology*, **53**(1), 68–81, https://doi.org/10.5741/gems.53.1.68.

Lu, T. & Sunagawa, I. 1990. Structure of Brazil twin boundaries in amethyst showing Brewster fringes. *Physics and Chemistry of Minerals*, **17**(3), 207–211, https://doi.org/10.1007/bf00201451.

Notari, F., Boillat, P.-Y. & Caplan, C. 2001. Quartz α-SiO_2: Discrimination des améthystes et citrines naturelles et synthétiques. *Revue de Gemmologie A.F.G.*, No. 141/142, 75–80.

Schmetzer, K. 1987. Microscopic observation of twinning microstructure in natural amethyst. *Neues Jahrbuch für Mineralogie, Monatshefte*, No. 1, 8–15.

Schmetzer, K. 2017. Distinction of natural and synthetic ametrine by microscopic examination—A practical approach. *Journal of Gemmology*, **35**(6), 506–529, https://doi.org/10.15506/JoG.2017.35.6.506.

Schmetzer, K. & Bernhardt, H.J. 2002. Star garnets from Ilakaka, Madagascar. *Australian Gemmologist*, **21**(5), 202–206.

Schmetzer, K. & Glas, M. 2003. Multi-star quartzes from Sri Lanka. *Journal of Gemmology*, **28**(6), 321–332, https://doi.org/10.15506/JoG.2003.28.6.321.

Schmetzer, K. & Krzemnicki, M. 2006. The orientation and symmetry of light spots and asterism in rose quartz spheres from Madagascar. *Journal of Gemmology*, **30**(3), 183–191, https://doi.org/10.15506/JoG.2006.30.3.183.

Schmetzer, K. & Steinbach, M.P. 2022. Gem News International: Three-rayed asterism in quartz. *Gems & Gemology*, **58**(2), 249–252.

Schmetzer, K. & Steinbach, M.P. 2023. Gem Notes: Three-rayed asterism in quartz: A multi-star network. *Journal of Gemmology*, **38**(6), 552–553, https://doi.org/10.15506/JoG.2023.38.6.552.

Shelley, D. 1985. *Optical Mineralogy*. Elsevier, New York, New York, USA, 321 pp.

Steinbach, M.P. 2017. *Asterism: Gems with a Star*. MPS Publishing and Media, Idar-Oberstein, Germany, 896 pp. (see pp. 649–651).

Sunagawa, I., Iwasaki, H. & Iwasaki, F. 2009. Morphology of natural quartz crystals. *In*: *Growth and Morphology of Quartz Crystals Natural and Synthetic*. Terrapub Scientific Publishing Company, Tokyo, Japan (see chapter 6, pp. 125–132).

Walcott, A.J. 1937. Asterism in garnet, spinel, quartz and sapphire. *Geological Series of Field Museum of Natural History*, **7**(3), 39–57, https://doi.org/10.5962/bhl.title.3353.

Weibel, M. 1982. Wie entsteht der Stern? Asterismus und Chatoyance bei Edelsteinen. *Lapis*, **7**(10), 25–27, 30, 38.

The Authors

Prof. Jean-Pierre Gauthier and Jacques Fereire
Centre de Recherches Gemmologiques, Laboratoire de Gemmologie, U.F.R. des Sciences et des Techniques, Université de Nantes, 2, rue de la Houssinière, 44072 Nantes Cedex 3, France

Dr Emmanuel Fritsch FGA
Institut des Matériaux Jean Rouxel CNRS (UMR 6502), University of Nantes, BP 32229, F-44322, Nantes Cedex 3, France
Email: emmanuel.Fritsch@cnrs-imn.fr

Thanh Nhan Bui
Rue du Compas, 47/4, 1070 Brussels, Belgium